JACS
JOURNAL OF THE AMERICAN CHEMICAL SOCIETY
Article
Cite This: J. Am. Chem. Soc. 2018, 140, 1438−1446
pubs.acs.org/JACS

Chemical Design of Both a Glutathione-Sensitive Dimeric Drug Guest and a Glucose-Derived Nanocarrier Host to Achieve Enhanced Osteosarcoma Lung Metastatic Anticancer Selectivity

Lu Su,[‡,†] Richen Li,[‡,†] Sarosh Khan,[†] Ryan Clanton,[§] Fuwu Zhang,[†] Yen-Nan Lin,[†,#] Yue Song,[†] Hai Wang,[†] Jingwei Fan,[†] Soleil Hernandez,[§] Andrew S. Butters,[§] Gamal Akabani,[§] Ronan MacLoughlin,[⊥,∥,▽] Justin Smolen,*[,†] and Karen L. Wooley*[,†]

[†]Departments of Chemistry, Chemical Engineering, and Materials Science & Engineering, Texas A&M University, College Station, Texas 77842, United States

[#]College of Medicine, Texas A&M University, Bryan, Texas 77807, United States

[§]Departments of Nuclear Engineering and Veterinary Integrative Biosciences and Texas A&M Institute for Preclinical Studies, Texas A&M University, College Station, Texas 77842, United States

[⊥]Aerogen, IDA Business Park, Dangan, Galway, Ireland.

[∥]School of Pharmacy, Royal College of Surgeons, Dublin, Ireland.

[▽]School of Pharmacy and Pharmaceutical Sciences, Trinity College, Dublin, Ireland

Supporting Information

ABSTRACT: Although nanomedicines have been pursued for nearly 20 years, fundamental chemical strategies that seek to optimize both the drug and drug carrier together in a concerted effort remain uncommon yet may be powerful. In this work, two block polymers and one dimeric prodrug molecule were designed to be coassembled into degradable, functional nanocarriers, where the chemistry of each component was defined to accomplish important tasks. The result is a poly(ethylene glycol) (PEG)-protected redox-responsive dimeric paclitaxel (diPTX)-loaded cationic poly(D-glucose carbonate) micelle (**diPTX@CPGC**). These nanostructures showed tunable sizes and surface charges and displayed controlled PTX drug release profiles in the presence of reducing agents, such as glutathione (GSH) and dithiothreitol (DTT), thereby resulting in significant selectivity for killing cancer cells over healthy cells. Compared to free PTX and diPTX, **diPTX@CPGC** exhibited improved tumor penetration and significant inhibition of tumor cell growth toward osteosarcoma (OS) lung metastases with minimal side effects both *in vitro* and *in vivo*, indicating the promise of **diPTX@CPGC** as optimized anticancer therapeutic agents for treatment of OS lung metastases.

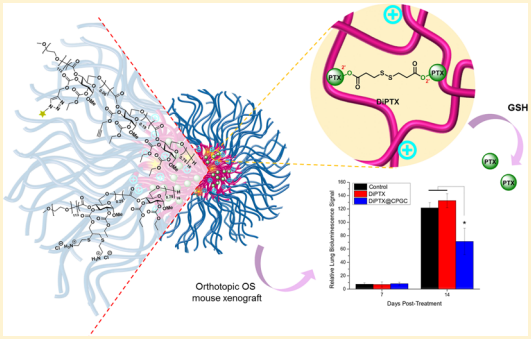

INTRODUCTION

Nanomedicine holds great potential to offer effective treatment against devastating diseases, by providing sustained release of significant quantities of therapeutic agents, especially when the route of administration allows for direct access to the diseased tissues.[1−5] Yet, rational design of the chemical structures of the drug and drug carrier are still needed to overcome several challenges influencing the success of *in vivo* studies, such as potential adverse effects of long-term accumulations of the nanocarriers, off-target toxicity of the therapeutics to normal tissues, and the limited ability of nanomedicines to penetrate tumor tissues at a potentially lethal concentration.[6−9]

Osteosarcoma (OS) is the most common primary cancer of bone in children and adolescents aged 10−20 years and the third most common cancer overall in adolescents, with no proven etiology and a high fatality rate (70% survival at 5 years for nonmetastatic patients and less than 30% for those presenting with metastasis).[10,11] The predominant site of metastasis is the lung, followed by other bones. Once micrometastases grow into recurrent, overt disease, tumors are often resistant to conventional chemotherapy, and unresectable recurrent disease is fatal.[12,13] Therefore, innovative strategies for prevention and treatment of the metastatic disease are of critical need. Recently, our group employed paclitaxel (PTX)-loaded polyphosphoester (PPE)-based polymeric micelles and shell cross-linked knedel-like nanoparticles (SCKs) as nanotherapeutics to treat OS lung metastases via aerosol-based delivery.[14] The strategy could provide distribution of nanocarriers throughout the lungs and achieve sufficient pulmonary drug concentrations while avoiding dilutional and systemic effects seen in intravenous (iv) administration, with

Received: October 27, 2017
Published: January 19, 2018

DOI: 10.1021/jacs.7b11462
J. Am. Chem. Soc. 2018, 140, 1438−1446

Scheme 1. Schematic Illustration of the Coassembly of Polymer 2 and Polymer 3 with diPTX and Redox-Responsive Drug Release to Enable Treatment of SJSA-1 Multicellular Tumor Spheroids (MCTSs) with Improved Penetration, Relative to Free Drug PTX and Prodrug diPTX

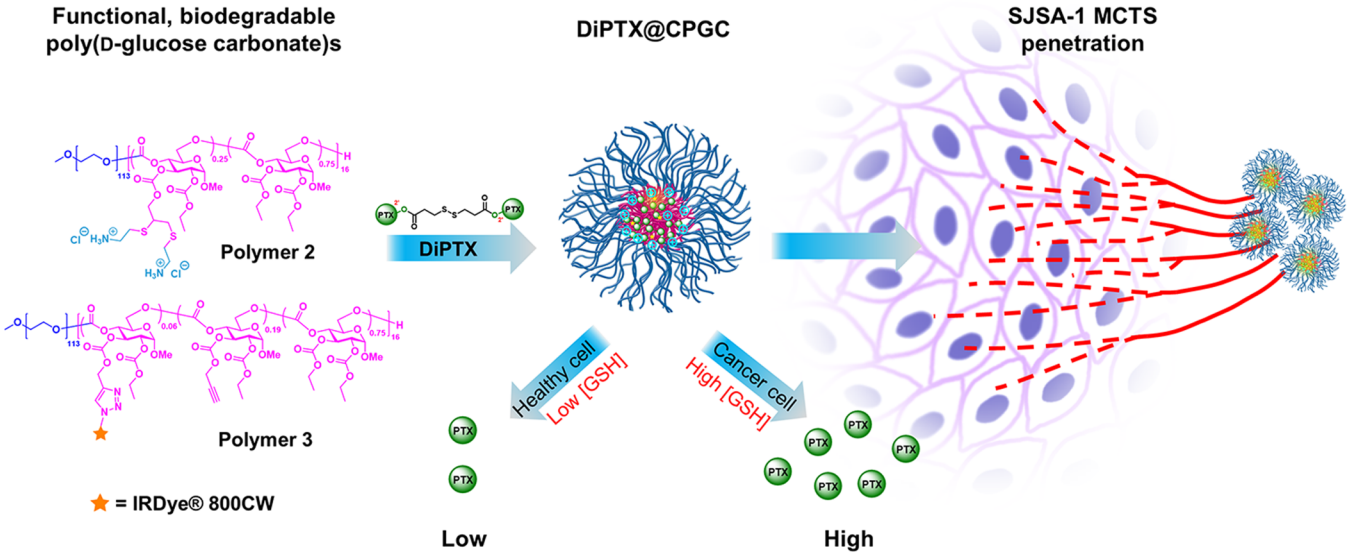

prolonged drug release and extended lung retention of the SCKs, owing to their cross-linked structure. However, safety concerns regarding the PPE degradation products, limited tissue and cell penetration ability, and off-target toxicity remained as key challenges. Therefore, in this report, an anticancer drug delivery system with optimized chemical structures was designed and developed, where the chemistry of each component is tailored to accomplish specific tasks. This system improves selectivity, enhances tumor penetration ability, and facilitates drug release in response to conditions associated with tumor microenvironment.

Nanoparticles derived from biodegradable polymers, such as polyesters,[15] polypeptides,[16] PPEs,[14,17,18] and polycarbonates,[19,20] have gained increasing interest for nanomedicines, which reduce the potential for long-term accumulation and associated adverse effects. Recently, our group employed functional glucose-derived polycarbonates (PGCs) to construct nanostructures with tunable sizes, surface charges, and morphologies that are, notably, capable of degradation into natural products, for example, glucose, carbon dioxide, and ethanol.[21,22] We expected that leveraging the PGC-derived nanostructures as nanocarriers would circumvent potential drawbacks of our previous PPE system,[14] namely, the production of ethylene glycol and phosphoric acid upon hydrolytic degradation, while maintaining the advantages of degradability, biocompatibility, and versatile functionality, such as for dye-labeling.[14] Furthermore, the steric bulk and increased hydrophobicity of the PGC backbone, relative to those of PPEs, were anticipated to enable extended drug release.

In order to access tumors for intracellular delivery within lung tissue via inhalation, the nanocarriers need to be capable of penetrating the diffusion and absorption barriers of the airway mucus,[23] lung epithelium,[24] and tumor stroma.[25] The diffusion/penetration capacity of drug carriers across these barriers is known to depend on the chemical composition, shape, and, in particular, size and surface properties of the nanocarriers,[26,27] and in this work these attributes were tuned to achieve optimal effects. Chan and co-workers reported the tumor permeation of PEGylated gold nanoparticles (GNPs)[28] and tiopronin-modified GNPs[29] to depend strongly on the size of the nanoparticles, where larger nanoparticles localized near the vasculature, while smaller nanoparticles diffused rapidly throughout the tumor matrix. Similarly, diffusion across respiratory mucus has been shown to be greatly restricted for particles larger than 100 nm.[30] Given the vital influence of particle size on their penetration ability, we targeted nanocarriers with desirable diameters of less than 30 nm.[4] Meanwhile, cationic charges were also shown to improve tumor penetration, due to nanoparticle-induced necrosis and resultant tumor cell density reduction,[31−34] which could be conveniently imparted into the PGC constructs via a facile thiol−yne click reaction. To mitigate undesirable characteristics of cationic polymers, including mucus binding and nonspecific cell toxicity,[15] PEG was conjugated as a hydrophilic shell.[35]

As the concentration of glutathione (GSH) in cancer cells can be several times higher than that in normal cells,[36,37] redox-responsive linkages have been extensively exploited in designing drug delivery vehicles and prodrugs capable of controlled, sustained drug release with reduction of off-target release and associated toxicity. For instance, disulfide-linked dimeric prodrugs of camptothecin,[38] doxorubicin,[38] and PTX[39,40] were recently encapsulated within amphiphilic polymers (i.e., methoxy poly(ethylene glycol)-*block*-polylactide) or PEGylated phospholipids to formulate prodrug-loaded micelles. Advantageous properties were observed with these constructs, including reducing agent dithiothreitol (DTT)-triggered *in vitro* drug release, enhanced anticancer efficacy, and reduced adverse effects. Therefore, disulfide-linked dimeric diPTX prodrugs were anticipated to allow for enhanced containment by the PGC-based nanocarrier, relative to PTX, owing to the larger size and redox-triggered sustained release. The cationic charges installed between the hydrophilic shell and hydrophobic core of the PGC nanocarriers were further anticipated to provide better access of the negatively charged GSH to the core domain and diPTX.

Coassembly of the redox-responsive diPTX prodrug with the cation- and PEG-modified PGCs yielded nanocarriers that facilitated precise control of intracellular drug delivery, which

DOI: 10.1021/jacs.7b11462
J. Am. Chem. Soc. 2018, 140, 1438−1446

Scheme 2. Synthesis of Polymer 1, PEG_{113}-*b*-[$PGC(EC)_{12}$-*co*-$PGC(EPC)_4$] by ROP of GC(EC) and GC(EPC), Followed by Postpolymerization Modification *via* a Thiol−yne Click Reaction with Cysteamine Hydrochloride to Prepare the Cationic Polymer 2, PEG_{113}-*b*-[$PGC(EC)_{12}$-*co*-$PGC(Cys)_4$], or *via* CuAAC to Afford NIR Dye-Labeled Polymer 3, PEG_{113}-*b*-[$PGC(EC)_{12}$-*co*-$PGC(EPC)_3$-*co*-$PGC(Dye)_1$][a]

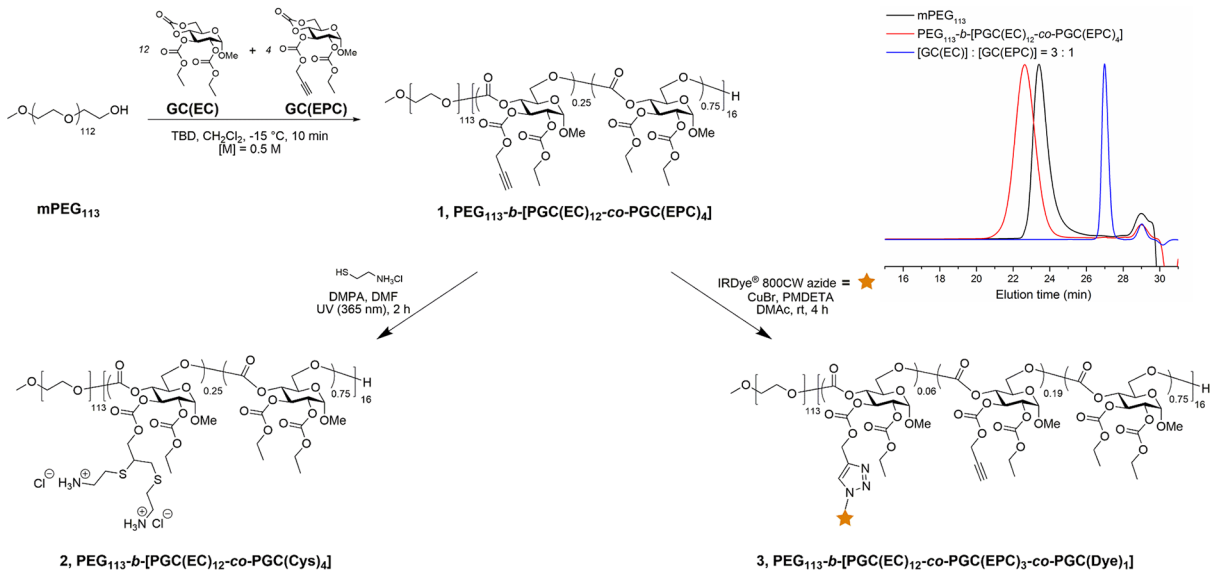

[a]Inset: Normalized SEC traces of polymer **1**, macroinitiator $mPEG_{113}$, and a mixture of the bicyclic carbonates GC(EC) and GC(EPC) with a molar ratio of 3:1 in THF.

holds great potential to finely tune drug release kinetics for beneficial anticancer activity with minimal undesired release in normal tissue. The anticancer efficacy as inhaled chemotherapeutics was evaluated both *in vitro* and *in vivo*, and the host−guest constructs exhibited improved tumor penetration and significant inhibition of tumor cell growth toward OS lung metastases with minimal side effects. These results demonstrate the promise of **diPTX@CPGC** as anticancer therapeutic agents for treatment of OS lung metastases.

RESULTS AND DISCUSSION

Rational Design of the diPTX-Loaded PGC Anticancer Drug Delivery System. Sugar-derived nanocarriers with near-infrared (NIR) labels and a cationic segment confined to either the interface between the hydrophilic shell and hydrophobic core or within the core were synthesized and used to encapsulate diPTX prodrugs with redox-responsive disulfide linkages (Scheme 1). In designing the nanocarrier structure to optimize cancer cell-specific drug delivery, PGC building blocks were selected due to their biocompatibility, degradability, functionality, and ability to assemble into versatile nanostructures with varied sizes, charges, and functionalities.[21] Cationic moieties were incorporated within the PEG-protected nanocarriers to allow negatively charged GSH to more readily access the core domain and to interact with the encapsulated diPTX, realizing preferential drug release in cancer cells with high GSH concentrations, while simultaneously increasing the tumor penetration ability and substantially reducing toxicity typically associated with cationic nanocarriers.[41,42] Once the disulfide bond in the diPTX prodrug is cleaved by a reducing agent, the thiol-terminated PTX derivative (PTX-SH) undergoes hydrolysis to release the free drug.[43] In addition, the dimeric size of the prodrug was expected to allow for enhanced containment by the nanocarrier to provide for sustained release. Coassembly of nonionic and cationic polymers was performed for the dual purposes of curtailing safety concerns associated with cationic polymers and tuning nanoparticle sizes.[41,42]

Synthesis and Postpolymerization Modification of Functional, Degradable PEG-*b*-PGCs. The functional and degradable diblock terpolymer **1**, PEG_{113}-*b*-[$PGC(EC)_{12}$-*co*-$PGC(EPC)_4$], was synthesized by rapid organocatalyzed ring-opening polymerization (ROP) of the bicyclic glucose carbonates methyl-2,3-*O*-ethyloxycarbonyl-4,6-*O*-carbonyl-*α*-D-glucopyranoside GC(EC) and methyl-2-*O*-ethyloxycarbonyl-3-*O*-propargyloxycarbonyl-4,6-*O*-carbonyl-*α*-D-glucopyranoside GC(EPC) at −15 °C in dichloromethane (DCM) with $mPEG_{113}$ as the macroinitiator and 1,5,7-triazabicyclo[4.4.0]-dec-5-ene (TBD) as the organocatalyst (Scheme 2). The monomer feed ratio [GC(EC)]/[GC(EPC)] was set to 3:1 to provide sufficient hydrophobicity and functionality. The reaction was quenched by addition of Amberlyst 15 H-form resin after 10 min, and size exclusion chromatography (SEC) (Scheme 2 inset) of the crude product showed no remaining monomers, indicating quantitative conversions of both monomers. The lower retention time of polymer **1** relative to $mPEG_{113}$ confirmed the successful chain extension to afford the expected diblock terpolymer. SEC further revealed monomodal molecular weight distribution and low dispersity ($Đ$ = 1.12), demonstrating the well-defined structure of the diblock terpolymer. The number-average molecular weight (M_n) and degree of polymerization (DP_n) of each monomer were calculated from the ^1H NMR spectrum (Figure S2) acquired after isolation of the polymer by precipitation, by comparing the integration of the CH_2CH_2O proton resonances (3.63 ppm) from the macroinitiator with the intensities of the resonances of protons attached to the anomeric carbons (5.01 ppm) and alkyne groups (2.59 ppm) in the PGC segment. Differential scanning calorimetry (DSC) revealed two glass transition temperatures (T_g) at −24 and 98 °C, corresponding to the mPEG and PGC segments, respectively.

DOI: 10.1021/jacs.7b11462
J. Am. Chem. Soc. 2018, 140, 1438−1446

The cationic terpolymer **2**, PEG_{113}-*b*-[$PGC(EC)_{12}$-*co*-$PGC(Cys)_4$], was prepared by postpolymerization modification of **1** via photoinitiated thiol−yne click reaction with a large excess of cysteamine hydrochloride (20 equiv relative to alkyne groups) (Scheme 2). The reaction mixture was dialyzed against nanopure water at 4 °C for 3 d to remove excess thiol and photoinitiator, then lyophilized to afford the product as a white powder in 95% yield. The presence of the cysteamine proton resonances at 2.66, 2.82, 2.99, and 7.88 ppm in the ^{1}H NMR spectrum and the disappearance of the alkyne carbon resonances at 78.91 and 77.70 ppm in the ^{13}C NMR spectrum indicated the consumption of the alkyne groups (Figures S4 and S5). Fourier transform infrared (FT-IR) spectroscopy further confirmed the consumption of the alkynes and the introduction of amine groups (Figure S8). Glass transitions of polymer **2** were observed at −25 and 92 °C in DSC thermograms, suggesting that self-assembled nanostructures would possess flexibility within a PEG shell (T_g = −25 °C) and stability of the PGC-based core (T_g = 92 °C).

The NIR-labeled polymer **3** was obtained by grafting the hydrophilic NIR dye, IRDye 800CW azide, to polymer **1** via copper-catalyzed alkyne−azide coupling (CuAAC) in *N*,*N*-dimethylacetamide (Scheme 2). The reaction mixture was filtered through a neutral alumina column and dialyzed against Chelex 100 resin in nanopure water for 4 d to remove copper species. Inductively coupled plasma-mass spectrometry (ICP-MS) confirmed the mass fraction of residual copper to be less than 10 ppm. The appearance of a new resonance corresponding to the triazole proton at 8.12 ppm (Figure S6) indicated successful conjugation of the IRDye 800CW to the polymer.

Preparation of diPTX-Loaded PGC Nanoparticles. PGC nanoparticles loaded with diPTX were obtained by utilizing the previously described nanoprecipitation method.[38,44] Briefly, a series of mixtures of the nonionic polymer **1** and cationic polymer **2** at predetermined mass ratios was first dissolved with diPTX (10 wt %) in DMSO and then added dropwise into nanopure water with vigorous stirring to form diPTX-loaded nanoparticles (concn (polymer) = 1 mg/mL) with 1 vol % DMSO. DiPTX loading was determined using high-performance liquid chromatography (HPLC), while the size, morphology, and surface charge were characterized by dynamic light scattering (DLS), atomic force microscopy (AFM), transmission electron microscopy (TEM), and electrophoretic light scattering (Figure 1 and Figure S9). HPLC revealed that the physical encapsulation of 10 wt % diPTX was highly effective, with efficiencies >98%. Although this standard loading of 10 wt % diPTX was employed, preliminary experiments were found to allow for higher diPTX loading, to levels of ca. 40 wt %. As depicted in Figure S9, DLS showed unimodal size distributions of all nanocarriers, suggesting the incorporation of polymer **1** and polymer **2** into the same nanostructures. The number-average hydrodynamic diameter ($D_{h(number)}$) of the diPTX-loaded nanoparticles increased from 20 ± 5 nm to 110 ± 28 nm (Figure 1a) as the mass ratio of the nonionic polymer **1** ($f_{polymer1}$) increased from 0 to 1, owing to the increased hydrophobic content. TEM and AFM images of diPTX-loaded nanoparticles with $f_{polymer1}$ of 0 and 0.2 showed circular structures with average diameters (D_{av}) of 23 ± 5 and 30 ± 8 nm, respectively (counting >50 nanoparticles) and heights of 4 ± 1 and 5 ± 1 nm (counting >50 nanoparticles), respectively, suggesting the formation of micellar structures. However, as the $f_{polymer1}$ increased above 0.2, the morphology

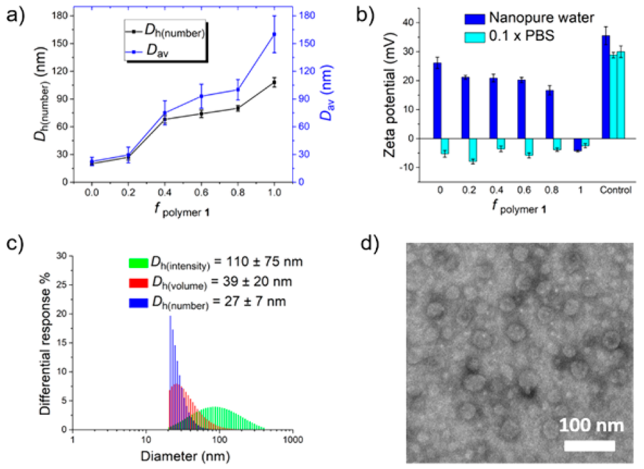

Figure 1. Characterization of **diPTX@CPGC**. (a) D_h and D_{av} as a function of $f_{polymer1}$, determined from DLS and TEM, respectively. (b) Zeta-potential of **diPTX@CPGC** in nanopure water and 0.1× PBS as a function of $f_{polymer1}$. Control zeta potential measurements were acquired on unloaded PGC(EC)-*b*-PGC(Cys) in nanopure water and 0.1× PBS and on physical mixtures of PGC(EC)-*b*-PGC(Cys) with $mPEG_{113}$ in 0.1× PBS, from left to right. (c) Number-, intensity- and volume-based hydrodynamic diameter of **diPTX@CPGC** ($f_{polymer1}$ = 0.2) in nanopure water measured by DLS. (d) TEM images of **diPTX@CPGC** ($f_{polymer1}$ = 0.2) negatively stained by 1 wt % phosphotungstic acid (PTA) aqueous solution (10 μL).

of the diPTX-loaded nanocarriers transformed from micelles to vesicles, indicated by the double layer structures observed in the TEM images, as well as the lower heights (3 ± 1 nm) in the AFM images (Figure S9). The hydrophobic diPTX prodrug was anticipated to be encapsulated in the core of the micelles or in the double layer of the vesicles. Zeta potential values (ξ) were characterized in nanopure water, 0.1× phosphate-buffered saline (PBS), and 10 mM $NaCl_{(aq)}$. As shown in Figure 1b, the ξ values measured for the five cationic nanocarriers were positive, ranging from 28 ± 2 mV to 16 ± 1 mV in nanopure water, while negative values of −5 ± 2 mV were obtained with the nonionic nanoparticles, a common phenomenon observed for neutral polymer assemblies.[45,46] In both 0.1× PBS and 10 mM $NaCl_{(aq)}$ (data not shown), all nanocarriers showed negative ξ (less than −10 mV), indicating PEG-like surface characteristics. As a control, the cationic PGC block polymer PGC(EC)-*b*-PGC(Cys) without the PEG segment (Scheme S1) showed positive ξ in all of these solutions, even when physically mixed with $mPEG_{113}$ at a mass ratio of 1:1, further confirming that the positively charged segment was protected by PEG. Recent studies suggest that cancer nanomedicines with smaller sizes exhibit enhanced *in vivo* performance due to greater tumor penetration.[32] Thus, micelles with $f_{polymer1}$ = 0.2 were chosen for subsequent release and cytotoxicity studies, as their size was less than 30 nm and ξ was relatively small (Figure 1c,d). Additionally, the small ratio of nonionic, alkyne-functionalized polymer **1** provided the possibility for further modification or cross-linking.

Evaluation of the Drug Release Kinetics. The drug release profiles of **diPTX@CPGC** were investigated in PBS in the presence or absence of reducing agents. The nonionic polymer PGC(EPC)-*b*-PGC(EC)-*g*-PEG_{2k} (Scheme S1) reported recently by our group[21] was utilized as a control to demonstrate the benefit of the positive charges residing at the core−shell interface on the diPTX release profile, as these

DOI: 10.1021/jacs.7b11462
J. Am. Chem. Soc. 2018, 140, 1438−1446

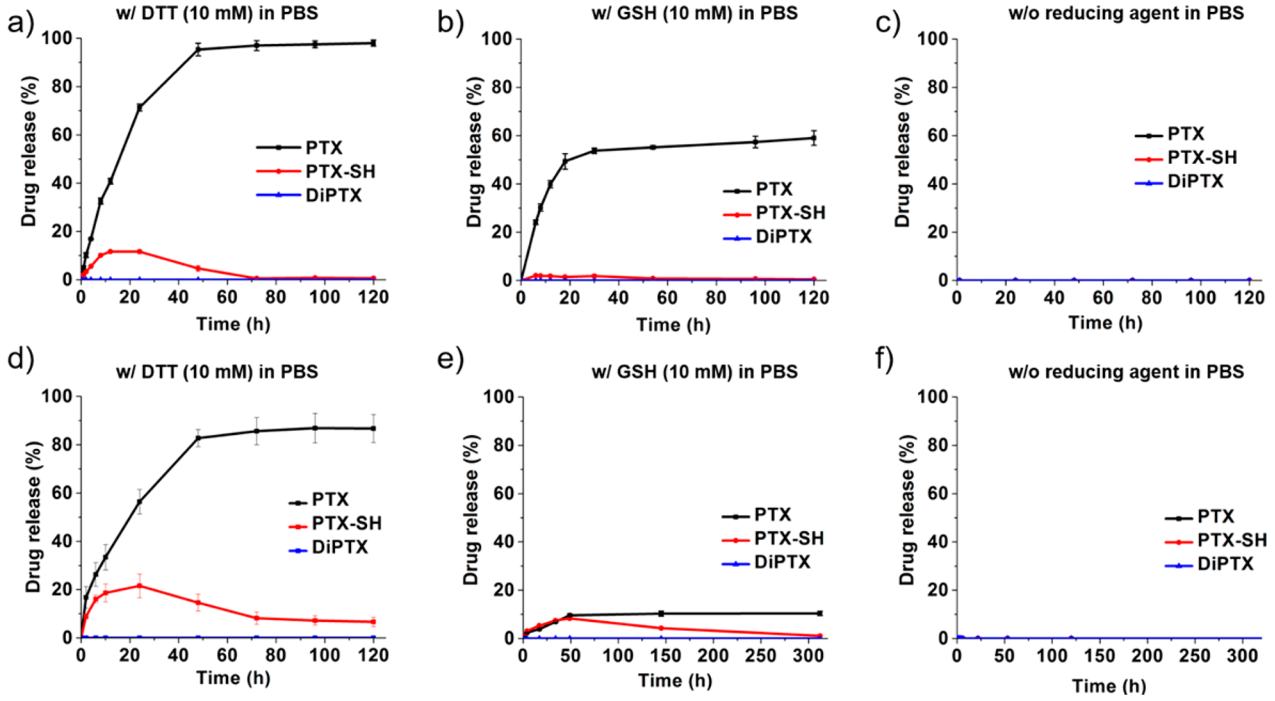

Figure 2. Release of PTX, PTX-SH, and diPTX from (a–c) diPTX-loaded cationic micelles ($f_{polymer1}$ = 0.2) and (d–f) diPTX-loaded PGC(EPC)-*b*-PGC(EC)-*g*-PEG_{2k} micelles at 37 °C in PBS containing (a, d) 10 mM DTT, (b, e) 10 mM GSH, and (c, f) no reducing agents, measured in triplicate. Error bars indicate standard deviation.

nanocarriers exhibited similar sizes and physicochemical properties, as characterized by DLS, TEM, AFM (Figure S10), and DSC. For the drug release studies, the micelle solutions were diluted to yield diPTX concentrations of ca. 100 μg/mL, which were confirmed by HPLC. The diPTX-loaded micelle solutions were then transferred into dialysis cassettes (molecular weight cutoff, MWCO, 10 kDa) and dialyzed against PBS (pH 7.4, 37 °C) containing either 10 mM DTT, 10 mM GSH, or no reducing agent. The drug release profiles were obtained by monitoring the concentrations of PTX, PTX-SH, and diPTX in the surrounding PBS solution as a function of time, and the percent drug release was calculated based on the PTX equivalents determined by HPLC. As depicted in Figure 2, no diPTX release was observed in any of the solutions, consistent with results recently reported for other dimeric prodrugs.[38] No significant release of PTX or PTX-SH was observed from either the cationic (Figure 2c) or nonionic PGC micelles in the absence of reducing agents (Figure 2f). In the presence of 10 mM DTT, **diPTX@CPGC** afforded sustained and controlled release of free PTX, which plateaued at almost complete drug release within 3 d, during which the concentration of PTX-SH increased initially and later dropped (Figure 2a). Similar sustained and controlled release of free PTX was achieved in 10 mM $GSH_{(aq)}$, reaching a plateau at ca. 55% release in 2 d (Figure 2b). The incomplete release may be due to reduced interaction of core-encapsulated diPTX with the relatively bulky reducing agent GSH. Yet, such release profiles, demonstrating relatively fast redox-responsive drug release over 2 d, followed by slower and more sustained drug release expected upon degradation of the nanoparticles in the human body, are anticipated to be quite beneficial for drug delivery. PTX release from the nonionic PGC micelles in the presence of 10 mM DTT was slightly slower than that from **diPTX@CPGC**, reaching a plateau at ca. 85% release within 3 d and 50% release in ca. 20 h (Figure 2d), slightly longer than the ca. 16 h required for 50% drug release from **diPTX@CPGC**. The PTX release rate from the nonionic PGC micelles in the presence of 10 mM GSH, however, was much slower with only ca. 10% PTX release in 2 d and no significant increase over time (Figure 2e), which may limit the potential of the nonionic formulations as efficient drug delivery systems. Taken together, the structure with positive charges confined either to the core–shell interface or within the core of the nanocarriers showed advantageous GSH-mediated drug release profiles over analogous nonionic nanocarriers. Thus, **diPTX@CPGC** were investigated further to evaluate anticancer efficacy *in vitro*.

Evaluation of Nanoparticle Toxicity. The *in vitro* cytotoxicity of **diPTX@CPGC** was evaluated in SJSA-1 and MC3T3 cell lines and compared to PTX (as a Taxol-mimicking formulation; Cremophor EL and ethanol, 1:1 v/v), diPTX (prepared similarly to the PTX formulation, Cremophor EL and ethanol, 1:1 v/v), and cationic PGC micelles without diPTX (Figure 3). The cationic micelles exhibited negligible toxicity in both cell lines below 0.2 mg/mL, indicating the protective effect of PEG, which has been reported to improve the biocompatibility of cationic nanoparticles.[21,46] In contrast, our earlier work with cationic PGC-based micelles, lacking a PEG shell, began showing reduction in cell viability at concentrations ranging from 0.05 to 0.1 mg/mL in RAW and MC3T3 cell lines.[21] In SJSA-1 cells (Figure 3a), **diPTX@CPGC** exhibited similar cytotoxicity to diPTX, which was slightly less toxic than the Taxol-mimicking formulation. The reduced cytotoxicity of the diPTX formulations, in comparison with PTX, may be attributed to the relatively slow free drug formation and release. As a result of the redox-responsive drug release mechanism, the cytotoxicity difference between diPTX and PTX was higher in noncancerous cells, which are expected to have a less reducing intracellular environment (Figure 3b). Accordingly, a higher IC_{50} value (0.14 μM PTX) was observed for diPTX relative to that measured for PTX (0.03 μM) in

DOI: 10.1021/jacs.7b11462
J. Am. Chem. Soc. 2018, 140, 1438–1446

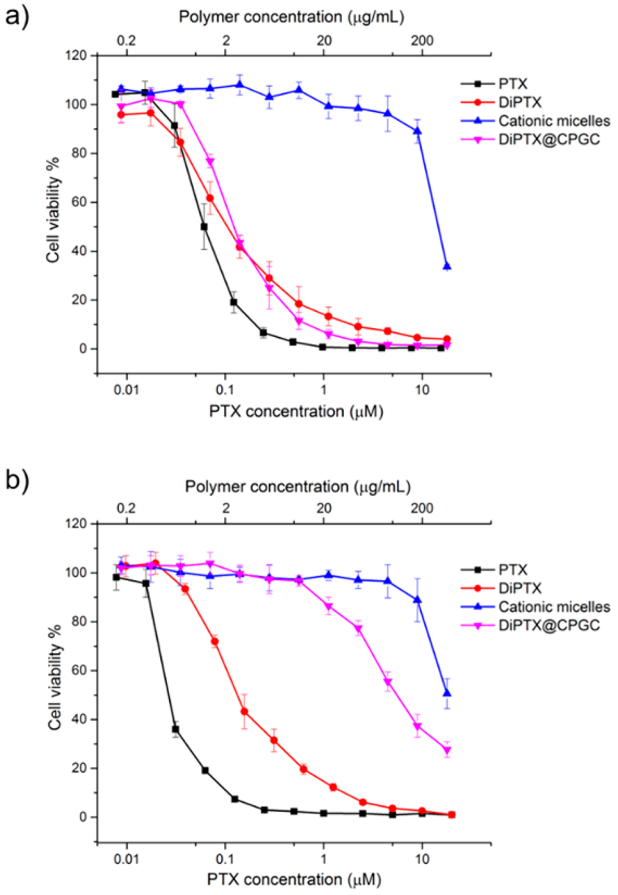

Figure 3. Cytotoxicity of PTX, diPTX, cationic PGC micelles, and **diPTX@CPGC** in (a) SJSA-1 and (b) MC3T3 cells. Cell viabilities are reported as an average of three measurements, and error bars represent standard deviation.

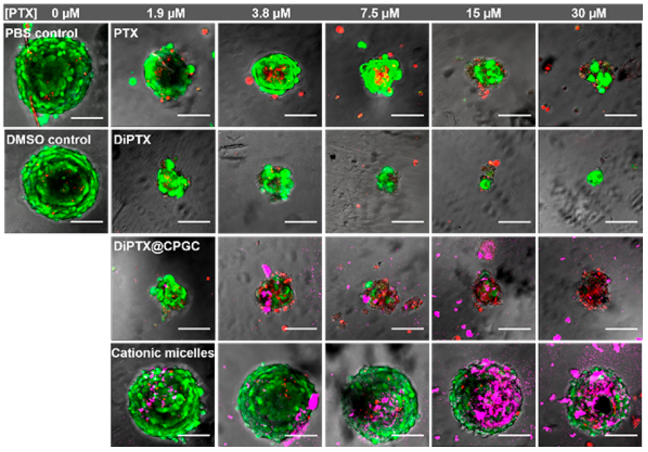

Figure 4. CLSM images of SJSA-1 MCTSs after treatment with PTX, diPTX, **diPTX@CPGC** containing 1.9−30 μM PTX, and cationic PGC micelles with equivalent polymer concentrations as used for the **diPTX@CPGC**, and PBS and DMSO controls (green, live cells; red, dead cells; purple, micelles). Scale bars represent 100 μm.

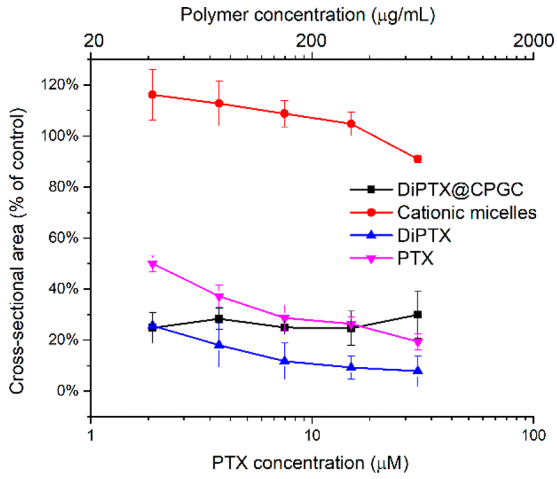

Figure 5. Growth inhibition of the SJSA-1 MCTSs by PTX, diPTX, **diPTX@CPGC**, and the cationic PGC micelles (no drug/prodrug) 7 d after addition of the formulations. Cross sectional areas are reported as an average of four measurements, and error bars represent standard deviation.

MC3T3 cells. The toxicity of **diPTX@CPGC** was further reduced in the MC3T3 cells compared to unencapsulated diPTX and PTX, with an IC_{50} value of ca. 5 μM, demonstrating selectivity for killing cancer cells over noncancerous cells. These studies, thus, confirm the advantages of **diPTX@CPGC** as cancer-selective agents and highlight the potential to reduce side effects in healthy cells without substantially sacrificing potency.

Nanoparticle Toxicity in SJSA-1 Spheroids. Multicellular tumor spheroids (MCTSs) are versatile three-dimensional models for studying tumor biology and screening cancer therapeutics due to the MCTSs possessing a similar morphology, biological microenvironment, and response to chemotherapeutics as solid tumors *in vivo*.[47−49] To test the effects of **diPTX@CPGC** on MCTSs, SJSA-1 human OS cancer cell-derived MCTSs were established on low-binding U-shaped microplates, incubated with micelles or controls, and evaluated as an *in vitro* model to assess penetration capability and cell proliferation inhibition (Scheme 1, Figure 4). The MCTS growth inhibition provided by the different formulations, that is, PTX, diPTX, **diPTX@CPGC**, and cationic PGC micelles (no drug/prodrug), was monitored by confocal laser scanning microscopy (CLSM), and the concentrations of PTX in the drug/prodrug formulations were determined by HPLC (Figure 5). PTX showed significant antitumor efficacy at concentrations from 1.9 to 30 μM PTX, with MCTS sizes reduced to ca. 50% of the controls at 1.9 μM PTX and ca. 20% at 30 μM PTX. In comparison, the reduction of SJSA-1 MCTSs upon treatment with the diPTX prodrug or **diPTX@CPGC** at 1.9 μM was similar, ca. 25% of the controls. At higher concentrations (3.8−30 μM PTX), the diPTX formulation reduced the MCTS size to the greatest extent, achieving ca. 10% of the control tumor size with formulations containing 30 μM PTX, while the **diPTX@CPGC** reduced the MCTSs to a similar extent (ca. 20−25%) for all concentrations. However, the live/dead staining results demonstrated that the remaining MCTSs incubated with diPTX still contained live cells at even the highest concentrations. In contrast, **diPTX@CPGC** appeared to kill all cells at the highest concentration, likely resulting from improved penetration into the core of the MCTS. Thus, the best killing performance was achieved with **diPTX@CPGC**, compared with the other two drug/prodrug formulations. The cationic PGC micelles without diPTX exhibited only slight anti-MCTS effect at the highest polymer concentration of 0.28 mg/mL, in which the amount of polymer

DOI: 10.1021/jacs.7b11462
J. Am. Chem. Soc. 2018, 140, 1438−1446

was equivalent to that in the 30 μM PTX formulation of **diPTX@CPGC**.

Nanoparticle Efficacy against OS Lung Metastases. An orthotopic xenograft mouse model was evaluated in order to determine the antitumor efficacy against OS lung metastases. NOD/SCID IL2-R-gamma −/− mice (aged 4−6 weeks) with established lung metastases were nebulized with different formulations, including Sham Control (PBS), diPTX prodrug (0.20 mg/mL in 95% PBS/5% DMSO), and **diPTX@CPGC** (0.20 mg/mL diPTX in PBS) (Figure S1). DMSO was necessary in order to obtain a stable suspension for the diPTX prodrug by itself, due to its highly hydrophobic nature. The lung bioluminescence signal of mice treated with micelles showed a ∼40% reduction in the growth of the lung metastases over the study, relative to control group, while the ones treated with free diPTX showed no reduction on the lung metastases (Figure 6a). Possibly due to enhanced penetration or better

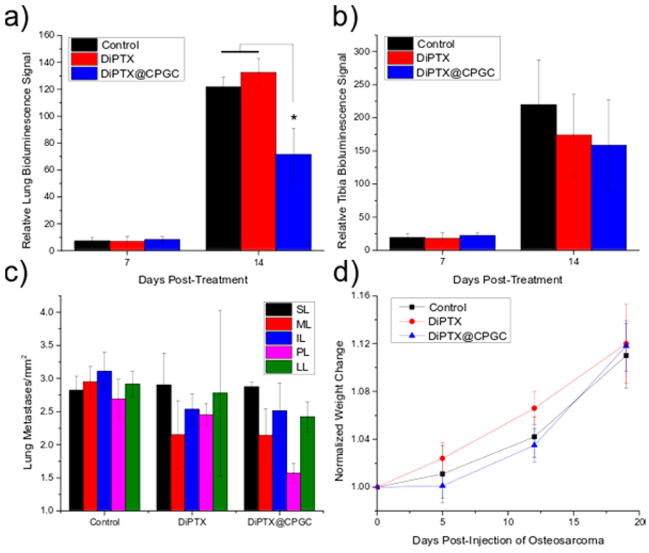

Figure 6. Relative OS tumor burden as measured by bioluminescence imaging, normalized to the baseline signal for each mouse, from (a) the lung metastases and (b) the primary tumor in the tibia after 7 and 14 d from the start of treatment. A significant reduction in tumor progression was observed in the lungs for the mice treated with **diPTX@CPGC** (p = 0.038 vs control, p = 0.0114 vs diPTX, one-way ANOVA with Tukey's post hoc comparison) but not with the free diPTX prodrug (p = 0.7839). No significant differences were observed for the tumor burden in the tibia. (c) Comparison of the metastases counted from histology of the different lung lobes *ex vivo* revealed a significant reduction in metastatic foci for the mice treated with **diPTX@CPGC** (p = 0.02 vs. control, two-way ANOVA with Tukey's post hoc comparison). SL, superior lobe; ML, middle lobe; IL, inferior lobe; PL, postcaval lobe; LL, left lung. (d) Tracking of the weight of the mice from the start of the study revealed no major differences among the groups.

retention in the lung, **diPTX@CPGC** exhibited a higher antitumor efficacy in the lung than did free diPTX. The micelles also had a nonsignificant trend toward lower tumor burden at the primary site of metastases over control and free diPTX (Figure 6b). Thus, the **diPTX@CPGC**, appeared to predominantly exhibit a loco-regional antitumor effect in the lungs, with limited systemic effect. *Ex vivo* imaging supported this conclusion, as high concentrations of micelles were found in the lungs but not other organs or primary tumor (Figures S12 and S13). While the lack of systemic antitumor effect may appear disadvantageous, we designed these nanocarriers for use as a potential replacement for the current osteosarcoma chemotherapy regimen, which is employed before and after surgical removal of the primary tumor in the bone.[50] Currently, systemic chemotherapy is employed regardless of detection of metastases and typically consists of high-dose methotrexate, cisplatin, and doxorubicin.[50] Systemic chemotherapeutic regimens, however, are associated with acute and chronic toxic effects,[51] including secondary malignancies.[52] Use of lung-specific anticancer therapy may allow for a reduction in systemic chemotherapy and thus a reduction in these adverse effects.[53]

The *in vivo* bioluminescence data were supported by *ex vivo* measurements of the number of metastases per mm^2 of lung tissue (Figure 6c) after the mice were euthanized 19 d from the injection of the SJSA-1 cells. Overall, **diPTX@CPGC** reduced the metastatic foci among the various lung segments (p = 0.02, two-way ANOVA with Tukey's post hoc comparison). Individual analysis of each lung segment revealed that some lung sections displayed a greater reduction than others, with the superior lobe of the right lung showing the least reduction. This lobe also appeared to receive the least amount of nanoparticles by lung area (Figure S12). Finally, the weights of the mice for the duration of the study (Figure 6d) showed no significant differences between the groups, suggesting that the diPTX prodrug and micelle formulations were well tolerated.

Evaluation of the NIR fluorescence signal for the lungs *ex vivo* (Figure S12) revealed that a relatively higher dose of micelles reached the left lung lobe, as compared to the lobes in the right lung, though all lobes showed a discernible signal. Microscopic examination of 20 μm lung slices via CLSM revealed that the micelles were well distributed throughout the various structures of the lung, including alveolar spaces, bronchi, blood vessels, and penetrating into tumor sites (Figure 7). Scans of the entire lung slices revealed that the micelles

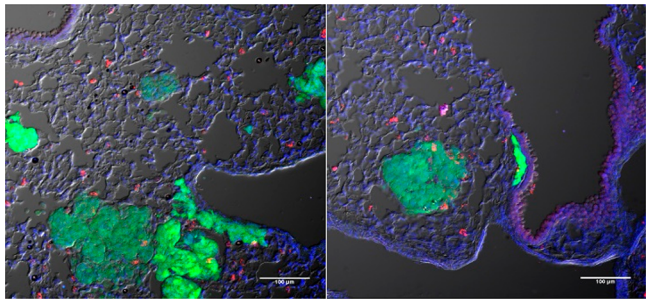

Figure 7. CLSM images of lung histological sections of mice treated with **diPTX@CPGC**. NIR-labeled **diPTX@CPGC** (red) were found to reach the tumor sites and penetrate into the GFP-expressing SJSA-1 tumors (green). Additionally, **diPTX@CPGC** aggregates were found in the alveolar spaces, near blood vessels, and along the surfaces of the bronchioles, as revealed by DAPI nuclear staining (blue) and Nomarski DIC transmitted light imaging (gray scale).

deposited primarily near the main branching airways, although micelles were found to extend to the periphery (Figures S14 and S15). Sections of the lungs with high deposition of nanoparticles also appeared to have fewer and smaller tumors, providing further evidence of localized anticancer effect. The deposition sites of the micelles appeared to show signs of aggregation (Figure 7), with large spots of high micelle concentration relative to the measured size of individual

DOI: 10.1021/jacs.7b11462
J. Am. Chem. Soc. 2018, 140, 1438−1446

particles. Similar aggregation patterns have been seen in other studies of lung delivery of nanoparticles.[23,54,55] The process and kinetics of this phenomenon and whether it is specific to certain cell types deserve further exploration. Importantly, the micelles did show an apparent ability to bypass the respiratory epithelium and access the tumors. Finally, only limited NIR signal was found in the other organs of the mice that were treated with micelle formulations (Figures S11 and S13), further confirming localized accumulation.

CONCLUSIONS

Two PGC-based block polymers and one dimeric PTX prodrug were designed to be coassembled into degradable, functional nanocarriers, where the chemistry of each component was defined to accomplish important tasks. The well-defined diblock terpolymer PEG-*b*-PGC(EC)-*co*-PGC(EPC) was synthesized by rapid ROP of glucose-derived monomers, with good biocompatibility, degradability, and versatile functionality. Cationic moieties were introduced by thiol−yne click modification of the PGC segment to construct nanocarriers with enhanced tumor penetration ability, while undesirable characteristics of cationic polymers were mitigated by the PEG shell. Disulfide-linked diPTX prodrug was designed to allow for redox-triggered release in cancer cells with high GSH concentration, where the negatively charged GSH can readily interact with encapsulated diPTX due to confined cationic charges in the shell−core interface or within core domain. In addition, enhanced nanocarrier containment of diPTX was achieved, relative to PTX, to provide for sustained release. A series of nanocarriers with different sizes, surface charges, and morphologies was constructed by tuning the mass ratio of the amphiphilic cationic PGC and an analogous NIR-labeled nonionic polymer employed in coassembly. Given their suitable size, zeta potential, and nanostructure, cationic PEG-*b*-PGC micelles with f_{polymer1} = 0.2 were selected for *in vitro* studies, which showed controlled and sustained *in vitro* PTX drug release in the presence of GSH or DTT. Cytotoxicity assays confirmed the biocompatibility of **diPTX@CPGC**, and significant selectivity of **diPTX@CPGC** for killing cancer cells over healthy cells. Studies in SJSA-1 MCTSs demonstrated improved tumor penetration ability and anticancer efficacy of **diPTX@CPGC** relative to Taxol-mimicking formulations. Therefore, the anticancer efficacy of **diPTX@CPGC** as inhaled chemotherapeutics was further evaluated in an orthotopic mouse model of human OS, with free diPTX and PBS as control groups. The lung bioluminescence signal of mice 14 d after treatment with **diPTX@CPGC** was significantly lower relative to the PBS controls, demonstrating their capability to slow the growth of lung metastases. Throughout the duration of the study, no significant differences were observed in the weights of the mice in the treatment and control groups, indicating the tolerance of the diPTX prodrug and the PGC micelles. The micelles distributed appreciably throughout various structures of the lung, demonstrated by the *ex vivo* studies. The *ex vivo* study results also confirmed a reduction of tumor growth after treatment with **diPTX@CPGC**, indicating the promise of **diPTX@CPGC** as optimized anticancer therapeutic agents for treatment of OS lung metastases.

ASSOCIATED CONTENT

Supporting Information

The Supporting Information is available free of charge on the ACS Publications website at DOI: 10.1021/jacs.7b11462.

Experimental methods and additional characterization data (PDF)

AUTHOR INFORMATION

Corresponding Authors

*justin.smolen@chem.tamu.edu
*wooley@chem.tamu.edu

ORCID

Karen L. Wooley: 0000-0003-4086-384X

Author Contributions

‡L.S. and R.L. contributed equally.

Notes

The authors declare no competing financial interest.

ACKNOWLEDGMENTS

This material is based upon work supported by the National Science Foundation (CHE-1610311). We also gratefully acknowledge financial support from the Robert A. Welch Foundation through the W. T. Doherty-Welch Chair in Chemistry (A-0001).

REFERENCES

(1) Elsabahy, M.; Wooley, K. L. *Chem. Soc. Rev.* **2012**, *41*, 2545.
(2) Dai, Y.; Xu, C.; Sun, X.; Chen, X. *Chem. Soc. Rev.* **2017**, *46*, 3830.
(3) Elsabahy, M.; Heo, G. S.; Lim, S.-M.; Sun, G.; Wooley, K. L. *Chem. Rev.* **2015**, *115*, 10967.
(4) Sun, Q. H.; Zhou, Z. X.; Qiu, N. S.; Shen, Y. Q. *Adv. Mater.* **2017**, *29*, 1606628.
(5) Sun, T. M.; Zhang, Y. S.; Pang, B.; Hyun, D. C.; Yang, M. X.; Xia, Y. N. *Angew. Chem., Int. Ed.* **2014**, *53*, 12320.
(6) Shi, J.; Kantoff, P. W.; Wooster, R.; Farokhzad, O. C. *Nat. Rev. Cancer* **2017**, *17*, 20.
(7) Chen, H.; Zhang, W.; Zhu, G.; Xie, J.; Chen, X. *Nat. Rev. Mater.* **2017**, *2*, 17024.
(8) Wilhelm, S.; Tavares, A. J.; Dai, Q.; Ohta, S.; Audet, J.; Dvorak, H. F.; Chan, W. C. W. *Nat. Rev. Mater.* **2016**, *1*, 16014.
(9) Minchinton, A. I.; Tannock, I. F. *Nat. Rev. Cancer* **2006**, *6*, 583.
(10) Meyers, P. A.; Schwartz, C. L.; Krailo, M. D.; Healey, J. H.; Bernstein, M. L.; Betcher, D.; Ferguson, W. S.; Gebhardt, M. C.; Goorin, A. M.; Harris, M.; Kleinerman, E.; Link, M. P.; Nadel, H.; Nieder, M.; Siegal, G. P.; Weiner, M. A.; Wells, R. J.; Womer, R. B.; Grier, H. E. *J. Clin. Oncol.* **2008**, *26*, 633.
(11) Ottaviani, G.; Jaffe, N. *The Epidemiology of Osteosarcoma*; Springer: Dordrecht, 2009.
(12) Bielack, S. S.; Kempf-Bielack, B.; Branscheid, D.; Carrle, D.; Friedel, G.; Helmke, K.; Kevric, M.; Jundt, G.; Kuhne, T.; Maas, R.; Schwarz, R.; Zoubek, A.; Jurgens, H. *J. Clin. Oncol.* **2009**, *27*, 557.
(13) Hughes, D. P. M. *Curr. Opin. Oncol.* **2009**, *21*, 332.
(14) Zhang, F.; Zhang, S.; Pollack, S. F.; Li, R.; Gonzalez, A. M.; Fan, J.; Zou, J.; Leininger, S. E.; Pavía-Sanders, A.; Johnson, R.; Nelson, L. D.; Raymond, J. E.; Elsabahy, M.; Hughes, D. M. P.; Lenox, M. W.; Gustafson, T. P.; Wooley, K. L. *J. Am. Chem. Soc.* **2015**, *137*, 2056.
(15) Zhou, J.; Liu, J.; Cheng, C. J.; Patel, T. R.; Weller, C. E.; Piepmeier, J. M.; Jiang, Z.; Saltzman, W. M. *Nat. Mater.* **2012**, *11*, 82.
(16) Cameron, N.; Deming, T. *Macromol. Biosci.* **2015**, *15*, 7.
(17) McKinlay, C. J.; Waymouth, R. M.; Wender, P. A. *J. Am. Chem. Soc.* **2016**, *138*, 3510.
(18) Zhang, F.; Khan, S.; Li, R.; Smolen, J. A.; Zhang, S.; Zhu, G.; Su, L.; Jahnke, A. A.; Elsabahy, M.; Chen, X.; Wooley, K. L. *Nanoscale* **2017**, *9*, 15773.
(19) Brannigan, R. P.; Dove, A. P. *Biomater. Sci.* **2017**, *5*, 9.
(20) Ekladious, I.; Liu, R.; Zhang, H.; Foil, D. H.; Todd, D. A.; Graf, T. N.; Padera, R. F.; Oberlies, N. H.; Colson, Y. L.; Grinstaff, M. W. *Chem. Sci.* **2017**, *8*, 8443.

DOI: 10.1021/jacs.7b11462
J. Am. Chem. Soc. 2018, 140, 1438−1446

(21) Su, L.; Khan, S.; Fan, J.; Lin, Y.-N.; Wang, H.; Gustafson, T. P.; Zhang, F.; Wooley, K. L. *Polym. Chem.* **2017**, *8*, 1699.
(22) Song, Y.; Chen, Y. C.; Su, L.; Li, R. C.; Letteri, R. A.; Wooley, K. L. *Polymer* **2017**, *122*, 270.
(23) Schneider, C. S.; Xu, Q.; Boylan, N. J.; Chisholm, J.; Tang, B. C.; Schuster, B. S.; Henning, A.; Ensign, L. M.; Lee, E.; Adstamongkonkul, P.; Simons, B. W.; Wang, S.-Y. S.; Gong, X.; Yu, T.; Boyle, M. P.; Suk, J. S.; Hanes, J. *Sci. Adv.* **2017**, *3*, e1601556.
(24) de Souza Carvalho, C.; Daum, N.; Lehr, C. M. *Adv. Drug Delivery Rev.* **2014**, *75*, 129.
(25) Chauhan, V. P.; Stylianopoulos, T.; Boucher, Y.; Jain, R. K. *Annu. Rev. Chem. Biomol. Eng.* **2011**, *2*, 281.
(26) Minchinton, A. I.; Tannock, I. F. *Nat. Rev. Cancer* **2006**, *6*, 583.
(27) Lock, L. L.; Reyes, C. D.; Zhang, P.; Cui, H. *J. Am. Chem. Soc.* **2016**, *138*, 3533.
(28) Perrault, S. D.; Walkey, C.; Jennings, T.; Fischer, H. C.; Chan, W. C. W. *Nano Lett.* **2009**, *9*, 1909.
(29) Huang, K. Y.; Ma, H. L.; Liu, J.; Huo, S. D.; Kumar, A.; Wei, T.; Zhang, X.; Jin, S. B.; Gan, Y. L.; Wang, P. C.; He, S. T.; Zhang, X. N.; Liang, X. J. *ACS Nano* **2012**, *6*, 4483.
(30) Murgia, X.; Pawelzyk, P.; Schaefer, U. F.; Wagner, C.; Willenbacher, N.; Lehr, C.-M. *Biomacromolecules* **2016**, *17*, 1536.
(31) Yim, H.; Park, S. J.; Bae, Y. H.; Na, K. *Biomaterials* **2013**, *34*, 7674.
(32) Bugno, J.; Hsu, H.-J.; Pearson, R. M.; Noh, H.; Hong, S. *Mol. Pharmaceutics* **2016**, *13*, 2155.
(33) Li, H.-J.; Du, J.-Z.; Liu, J.; Du, X.-J.; Shen, S.; Zhu, Y.-H.; Wang, X.; Ye, X.; Nie, S.; Wang, J. *ACS Nano* **2016**, *10*, 6753.
(34) Punia, A.; Lee, K.; He, E.; Mukherjee, S.; Mancuso, A.; Banerjee, P.; Yang, N. L. *Int. J. Mol. Sci.* **2015**, *16*, 23867.
(35) Xu, Q. G.; Ensign, L. M.; Boylan, N. J.; Schon, A.; Gong, X. Q.; Yang, J. C.; Lamb, N. W.; Cai, S. T.; Yu, T.; Freire, E.; Hanes, J. *ACS Nano* **2015**, *9*, 9217.
(36) Diehn, M.; Cho, R. W.; Lobo, N. A.; Kalisky, T.; Dorie, M. J.; Kulp, A. N.; Qian, D.; Lam, J. S.; Ailles, L. E.; Wong, M.; Joshua, B.; Kaplan, M. J.; Wapnir, I.; Dirbas, F. M.; Somlo, G.; Garberoglio, C.; Paz, B.; Shen, J.; Lau, S. K.; Quake, S. R.; Brown, J. M.; Weissman, I. L.; Clarke, M. F. *Nature* **2009**, *458*, 780.
(37) Estrela, J. M.; Ortega, A.; Obrador, E. *Crit. Rev. Clin. Lab. Sci.* **2006**, *43*, 143.
(38) Cai, K.; He, X.; Song, Z.; Yin, Q.; Zhang, Y.; Uckun, F. M.; Jiang, C.; Cheng, J. *J. Am. Chem. Soc.* **2015**, *137*, 3458.
(39) Pei, Q.; Hu, X.; Liu, S.; Li, Y.; Xie, Z.; Jing, X. *J. Controlled Release* **2017**, *254*, 23.
(40) Han, X.; Chen, J.; Jiang, M.; Zhang, N.; Na, K.; Luo, C.; Zhang, R.; Sun, M.; Lin, G.; Zhang, R.; Ma, Y.; Liu, D.; Wang, Y. *ACS Appl. Mater. Interfaces* **2016**, *8*, 33506.
(41) de Planque, M. R. R.; Aghdaei, S.; Roose, T.; Morgan, H. *ACS Nano* **2011**, *5*, 3599.
(42) Leroueil, P. R.; Berry, S. A.; Duthie, K.; Han, G.; Rotello, V. M.; McNerny, D. Q.; Baker, J. R.; Orr, B. G.; Banaszak Holl, M. M. *Nano Lett.* **2008**, *8*, 420.
(43) Zou, J.; Zhang, F.; Zhang, S.; Pollack, S. F.; Elsabahy, M.; Fan, J.; Wooley, K. L. *Adv. Healthcare Mater.* **2014**, *3*, 441.
(44) Pinto Reis, C.; Neufeld, R. J.; Ribeiro, A. J.; Veiga, F. *Nanomedicine* **2006**, *2*, 8.
(45) Su, L.; Zhang, W. Y.; Wu, X. L.; Zhang, Y. F.; Chen, X.; Liu, G. W.; Chen, G. S.; Jiang, M. *Small* **2015**, *11*, 4191.
(46) Zhang, S.; Zou, J.; Zhang, F.; Elsabahy, M.; Felder, S. E.; Zhu, J.; Pochan, D. J.; Wooley, K. L. *J. Am. Chem. Soc.* **2012**, *134*, 18467.
(47) Lazzari, G.; Couvreur, P.; Mura, S. *Polym. Chem.* **2017**, *8*, 4947.
(48) Friedrich, J.; Seidel, C.; Ebner, R.; Kunz-Schughart, L. A. *Nat. Protoc.* **2009**, *4*, 309.
(49) Mehta, G.; Hsiao, A. Y.; Ingram, M.; Luker, G. D.; Takayama, S. *J. Controlled Release* **2012**, *164*, 192.
(50) Harrison, D. J.; Geller, D. S.; Gill, J. D.; Lewis, V. O.; Gorlick, R. *Expert Rev. Anticancer Ther.* **2018**, *18*, 39.
(51) Hattinger, C. M.; Pasello, M.; Ferrari, S.; Picci, P.; Serra, M. *Expert Opin. Emerging Drugs* **2010**, *15*, 615.
(52) Janeway, K. A.; Grier, H. E. *Lancet Oncol.* **2010**, *11*, 670.
(53) Abdelaziz, H. M.; Gaber, M.; Abd-Elwakil, M. M.; Mabrouk, M. T.; Elgohary, M. M.; Kamel, N. M.; Kabary, D. M.; Freag, M. S.; Samaha, M. W.; Mortada, S. M.; Elkhodairy, K. A.; Fang, J.-Y.; Elzoghby, A. O. *J. Controlled Release* **2018**, *269*, 374.
(54) Taratula, O.; Kuzmov, A.; Shah, M.; Garbuzenko, O. B.; Minko, T. *J. Controlled Release* **2013**, *171*, 349.
(55) Mastorakos, P.; da Silva, A. L.; Chisholm, J.; Song, E.; Choi, W. K.; Boyle, M. P.; Morales, M. M.; Hanes, J.; Suk, J. S. *Proc. Natl. Acad. Sci. U. S. A.* **2015**, *112*, 8720.

DOI: 10.1021/jacs.7b11462
J. Am. Chem. Soc. 2018, 140, 1438−1446